AN INSTANTANEOUS RIGID FORCE MODEL FOR 3-AXIS BALL-END MILLING OF SCULPTURED SURFACES

M. H. Sadeghi and R. Salami Naserian

Mechanical Engineering Department, Tarbiat Modarres University
Tehran, Iran, sadeghim@modares.ac.ir

H. Haghighat

Mechanical Engineering Department, Razi University
Kermanshah, Iran

(Received: October 3, 2002 – Accepted in Revised Form: October 28, 2003)

Abstract An instantaneous rigid force model for prediction of cutting forces in ball-end milling of sculptured surfaces is presented in this paper. A commercially available geometric engine is used to represent the cutting edge, cutter and updated part geometries. The cutter used in this work is an insert type ball-end mill. Intersecting an inclined plane with the cutter ball nose generates the cutting edge. Immersion geometry along the tool path is computed using the contact face between the ball-end mill and the solid model of the updated part. The engaged portion of the cutting edge is divided into small differential oblique cutting edge segments. Friction, shear angles and shear stresses are obtained from orthogonal cutting data available in the open literature. For each tool rotational position, the cutting force components are calculated by summation of the differential cutting forces. The developed model has been verified through experiments performed on several workpieces with different front and side angles. The predicted cutting forces have shown good agreement with experimental results. The developed model can be used as an efficient tool for predicting cutting performance in ball-end milling of sculptured surfaces of dies and moulds.

Key Words Ball-End Milling, Cutting Force, Die and Mould Machining

چکیده در این مقاله یک روش برای مدل سازی نیروهای ماشین کاری در فرایند فرز کاری با ابزار فرز سرکروی در ماشین کاری سطوح قالبها بیان شده است . مدل ارائه شده دارای قابلیت تخمین نیروهای ماشین کاری برای شرایط ماشین کاری مختلف می باشد . برای نمایش لبه برش ، ابزار و قطعه در حال ماشین کاری از یک نرم افزار مدل سازی هندسی (ACIS) استفاده شده است . قسمت در حال برش لبه برش در هر موقعیت زاویه ای ابزار تقاطع منحنی لبه برشی با لبه های وجه تماس بین ابزار و قطعه در حال ماشین کاری محاسبه میشوند . برای محاسبه نیروهای وارد بر ابزار ، قسمت در حال ماشین کاری لبه برش به المان های کوچک تقسیم شده و فرایند ماشین کاری در هر المان به صورت فرایند ماشین کاری مایل شده و نیروهای کل وارد بر ابزار در هر زاویه دوران ابزار از جمع نیروهای المانی محاسبه شده اند . آزمایش های مختلف نیز برای بررسی صحت و سقم نتایج شبیه سازی انجام شده است.

1. INTRODUCTION

The ball-end milling process is used extensively for machining of free form surfaces of dies and moulds used in automotive, aerospace, and appliances industries. Cutting force is one of the most important process parameters, determining performance of this machining operation. Cutting force is related to various process features such as tool deflection, tool breakage or chipping, excessive tool wear and vibration. It is therefore necessary to develop a force model that can accurately characterize the performance of the ball-end mill as it removes workpiece material in 3D curved surface machining.

Hosoi [1] first studied the cutting operation of the ball-end mills. He showed experimentally that a spiral shaped cutting edge could perform highly productive machining without edge chipping. In this work, no attempt was made to study the mechanics of cutting in the ball-end milling process. The down milling situation was found most advantageous for the spiral shaped cutting edge, since it reduced the

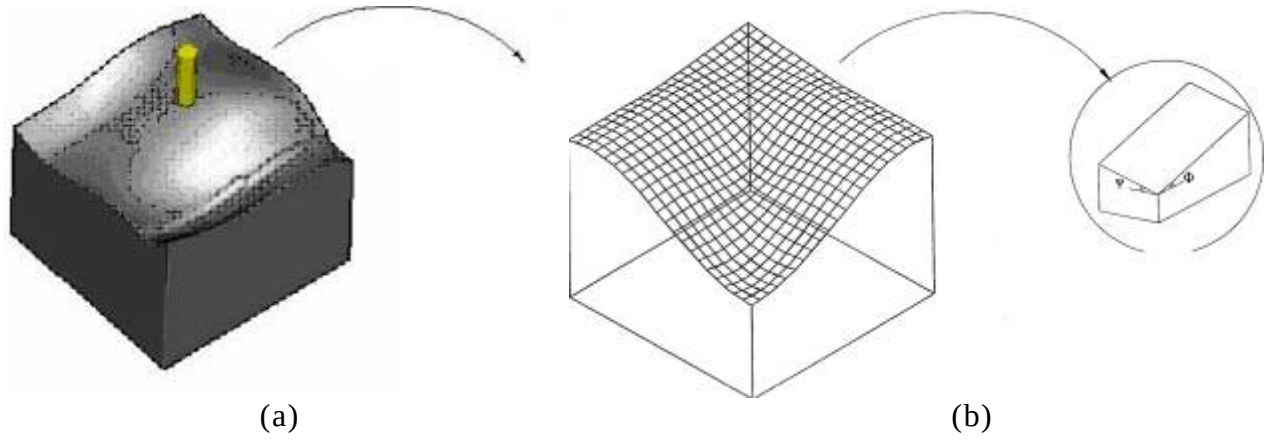

Figure 1. (a) Sculptured surface (b) An element of sculptured surface.

shock at the edge engagement as well as cutting force. Several authors have previously studied the issue of estimating forces in ball-end milling. Yang and Park introduced a force model to predict the cutting forces in ball-end milling process [2]. In this model, an orthogonal cutting theory was applied to the plane of the cutting velocity and the chip velocity at an arbitrary point on the cutting edge. The development of the force model was based on an analysis of the cutting geometry of the ball-end mill with plane rake faces. Hence, the cutting edge geometry was simplified as a function of the normal rake angle of the plane rake face and the position of the cutting edge in the spherical coordinate system. This model was experimentally validated for light immersions only. Feng and Meng introduced a two-component mechanistic force model that considered local cutting mechanics of differential cutting edges by introducing the force coefficient *kt and *kr as polynomials of the axial depth of cut [3]. The cutter considered was a constant lead ball-end mill. Owing to the empirical nature of that model, a separate set of experiments was required to identify the numerical values of the empirical mode parameters for the particular workpiece-cutter combination. Abrari and Elbestawi have developed a closed form force model for flat and ball-end mills [4]. In this model, a set of closed form functions are introduced for the projected areas of chip load on the reference co-ordinate planes. A pair of cutting forces, normal and tangential, is associated with each projected area. An average specific pressure matrix relates the projected areas to two components of cutting forces. Yucessan and Altintas considered the normal and friction forces on both the rake and clearance faces of a constant lead ball-end mill [5]. They assumed that the loads on the rake face are proportional to the uncut chip thickness area, and the loads on the flank face are concentrated on the in-cut portion of the cutting edge. They also assumed average values for chip flow angle and cutting coefficient along the cutting edge. Calibration and verification of their model was limited to simple two-dimensional cases (i.e. slotting). Lee and Altintas introduced a force model using orthogonal cutting data for a constant lead cutter [6]. The helical flutes were divided into small differential oblique cutting edge segments. The orthogonal cutting parameters are carried to oblique milling edge geometry using the classical oblique transformation method. Model verification was limited to simple cases only (i.e. slotting). All the force models introduced above were applicable to ball-end milling of horizontal planes only. Imani, Sadeghi, and Elbestawi developed a mechanistic force model that was applicable to ball-end milling of non-horizontal planes [7]. They used a commercial solid modeler for extracting the geometric information required for the physical simulation. The cutting forces were calculated as the summation of normal and friction forces acting on the rake face and the cutting edge. The differential forces acting on the rake face were assumed to be proportional to the differential chip contact area and the chip contact length was equal to twice that of the undeformed chip thickness. They were also assumed that the

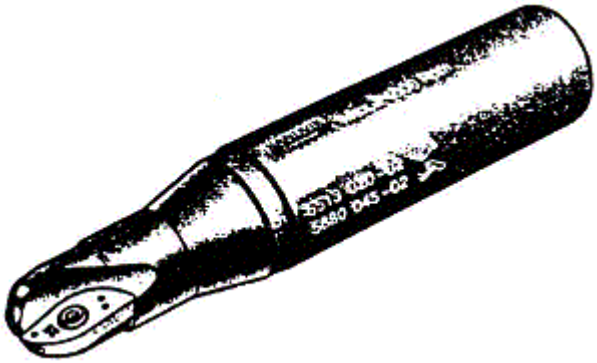

(a)

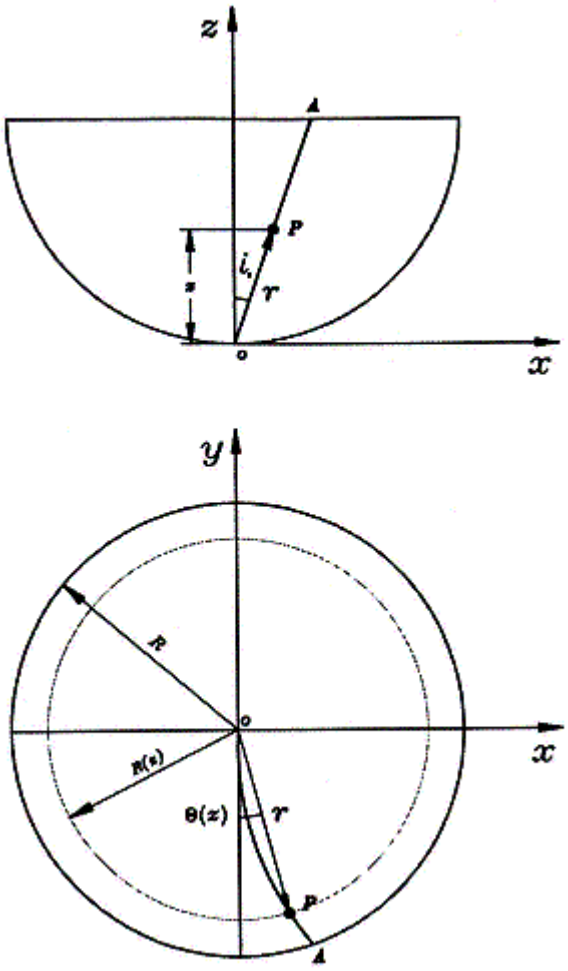

(b)

Figure 2. (a) An insert type ball end mill (b) Geometric model of an insert type ball-end mill.

friction force on the rake face acts in the chip flow direction, and that the variation of the chip flow angle in z direction had a linear characteristic with axial direction. The differential normal and frictional edge forces were proportional to the differential cutting-edge length. The cutting coefficients were identified from half immersion calibration tests. The mechanistic force model developed by Imani et al., although applicable to machining of non-horizontal surfaces depended on milling force coefficients determined from a set of experiments for each cutter geometry. By contrast the unified mechanics of cutting approach relies on an experimentally determined orthogonal cutting data base (i.e., shear angle, friction coefficient and shear stress), incorporating the tool geometrical variables, and milling model based on a generic oblique cutting analysis [8]. This approach eliminates the need for experimental calibration for each cutter geometry and can be applied to more complex cutter designs.

The aim of the present investigation is to develop a ball-end milling force model for predicting cutting forces in sculptured surfaces. Figure 1 shows a tilted plane with two angles, one relative to the x direction, Φ and the other, relative to the y direction, Ψ. The unified mechanics of cutting approach is extended for calculating cutting forces in this process. The cutter used in this work is an "insert type" ball-end mill. A commercially available solid modeler, ACIS [9], is used to represent the cutting edge, the cutter, and updated part geometries. Immersion geometry is computed using the contact face between the ball-end mill and the updated part. The engaged cutting edge portion, is divided into small elements. The geometric characteristics of a cutting edge element are analyzed to obtain the necessary parameters required for the oblique cutting force model. The cutting force components are calculated by summing up the differential cutting forces for each tool rotation step. The model is verified at different surface geometries (different Φ and Ψ angles) experimentally.

Organization of this paper is as follows: Geometric modeling of ball-end milling, which includes cutting edge, chip and immersion geometries are, discussed I section 2. In section 3, the modeling of cutting forces is discussed. In section 4, experimental verification of the force model is presented. Conclusion of the developed model is presented in section 5.

2. GEOMETRIC MODELLING

2.1. Tool Geometry Figure 2a shows the "insert

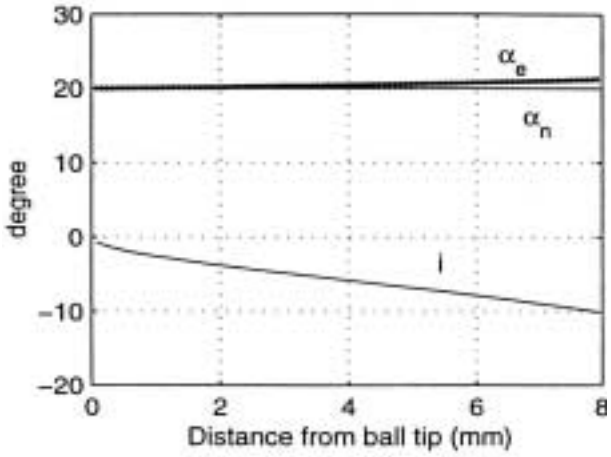

Figure 3. Variation of inclination angle i, normal rake angle a_e and effective rake angle a_n along axial direction for $a_n = 20^\circ$, $i_0 = 10^\circ$ and $R = 8mm$

type" ball-end mill used in this work. The cutting edge (OA in Figure 2b) is generated by the intersection of an inclined plane and the ball section of the cutter. The cutter radius in the $x-y$ plane at axial location z is;

$$R(z) = \sqrt{R^2 - (R-z)^2} \tag{1}$$

For an element at axial location z;

$$\sin\theta(z) = \frac{z\tan(i_0)}{R(z)} \tag{2}$$

where $\theta(z)$ is the angle between the ball tip $(z=0)$ and an element at axial location z. It is measured counter clockwise form the $-y$ axis (see Figure 2).

A vector r (OP in Figure 2b) is drawn from the Cartesian co-ordinate center to a point on the cutting edge, and is defined by;

$$r = R(z)\sin\theta(z)i - R(z)\cos\theta(z)j + zk \tag{3}$$

substituting Equation 2 in Equation 3 gives;

$$r = z\tan i_0 i - \sqrt{R^2(z) - (z\tan i_0)^2}\, j + zk \tag{4}$$

differentiating both sides of this equation results in;

$$dr = (\tan i_0 i - \frac{R(z)\frac{dR(z)}{dz} - z\tan^2 i_0}{\sqrt{R^2(z) - (z\tan i_0)^2}} j + k)dz \tag{5}$$

The length of an infinitesimal curved cutting edge element (ds) is computed by;

$$ds = \|dr\| = dz\sqrt{\tan^2 i_0 + \frac{[R(z)\frac{dR(z)}{dz} - z\tan^2 i_0]^2}{R^2(z) - (z\tan i_0)^2} + 1} \tag{6}$$

where,

$$\frac{dR(z)}{dz} = \frac{R-z}{R(z)} \tag{7}$$

the local inclination angle $i(z)$ is defined by;

$$ds\sin i(z) = R(z)d\theta \tag{8}$$

from Equation 2;

$$d\theta = \frac{\tan i_0[R(z) - z\frac{dR(z)}{dz}]}{R(z)\sqrt{R^2(z) - (z\tan i_0)^2}}dz \tag{9}$$

and therefore,

$$i(z) = \arcsin\frac{R(z)d\theta}{ds} \tag{10}$$

utilizing the Stabler's chip flow rule (i.e. $(\eta_c = i)$, the effective rake angle, α_e can be calculated from the following equation [10]:

$$\sin\alpha_e = \sin\alpha_n \sin i\cos\eta_c + \sin\eta_c \sin i \tag{11}$$

where α_n and η_c are the normal rake angle and the chip flow angle respectively. Figure 3 shows the variations of inclination angle (local helix angle) and effective rake angle along axial direction assuming $\alpha_n = 20^\circ$, $i_0 = 10^\circ$ and $R = 8mm$.

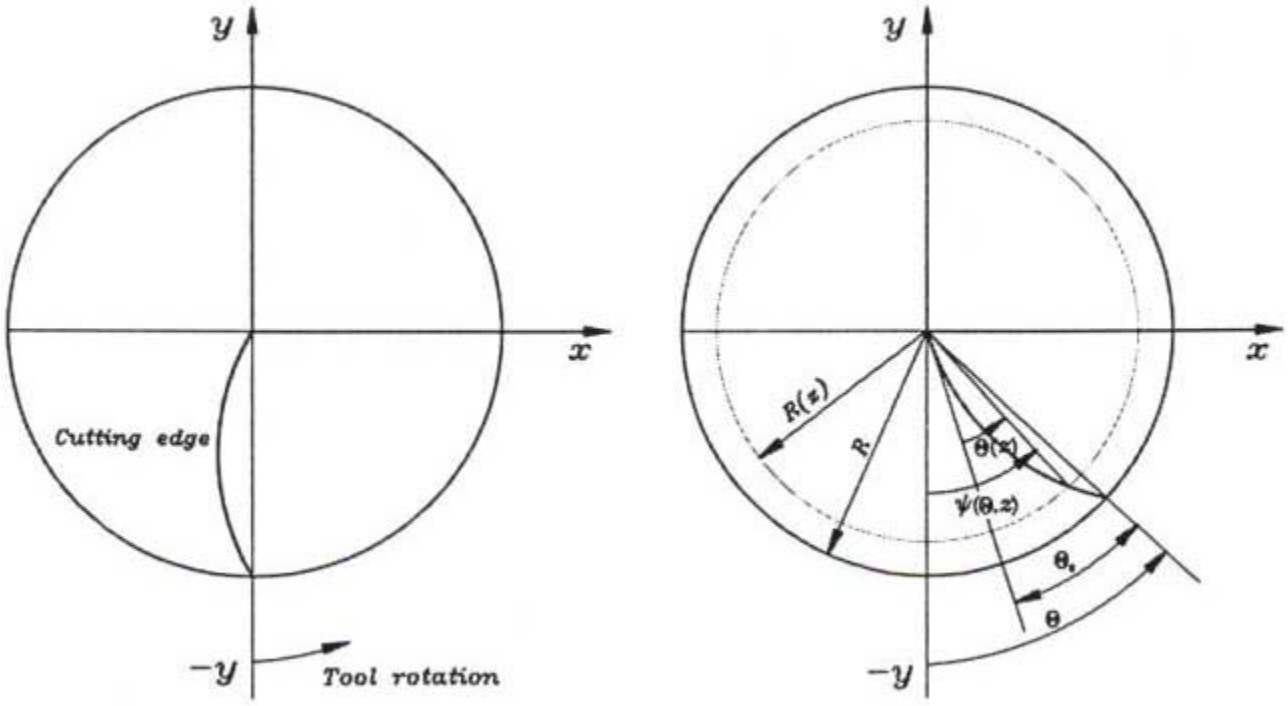

Figure 4. Position angle of an element on the cutting edge at axial location z.

A point on the flute j at height *z* is defined by its angular position $\psi(\theta, z)$ on the global co-ordinate system as shown in Figure 4;

$$\psi(\theta, z) = \theta + (j-1)\frac{2\pi}{N} - (\theta_0 - \theta(z)) \qquad (12)$$

where θ is the tool rotation angle about z axis and θ_0 is maximum angle between ball tip $(z = 0)$ and an element at axial location R. Then θ_0 can be calculated from Equation 2;

$$\theta_0 = \arcsin(\tan i_0) \qquad (13)$$

2.2. Undeformed Radial Chip Thickness Tooth path and radial chip thickness for milling process with horizontal feed directions have been studied by Martellotti [11,12]. For the case of 3-axis ball-end milling Lim et al. [13] considered the effect of vertical component of feed on chip thickness using the following relation;

$$t(\theta, z) = R_2(z) - R_1(z) + f_h \sin\psi(\theta, z) \qquad (14)$$

where f_h is a horizontal component of the feed along the tool path. $R_1(z)$ and $R_2(z)$ are the ball-nose radii at two successive positions in the same z value (Figure 5).

The difference between $R_1(z)$ and $R_2(z)$ is due to the vertical height difference f_v. Therefore, this difference can be approximated by;

$$R_2(z) - R_1(z) \cong -\frac{dR(z)}{dz} f_v \qquad (15)$$

substituting Equations 1, 7 and 15 in Equation 14 the chip thickness variation is as follows;

$$t(\theta, z) = \frac{R - z}{\sqrt{R^2 - (R-z)^2}} f_v + f_h \sin\psi(\theta, z) \qquad (16)$$

where, $f_v = f\sin\Phi, f_h = f\cos\Phi$, and Φ is the slope angle of the tool path shown in Figure 5.

2.3. Immersion Geometry Immersion geometry, required for force computation, is the engaged portion

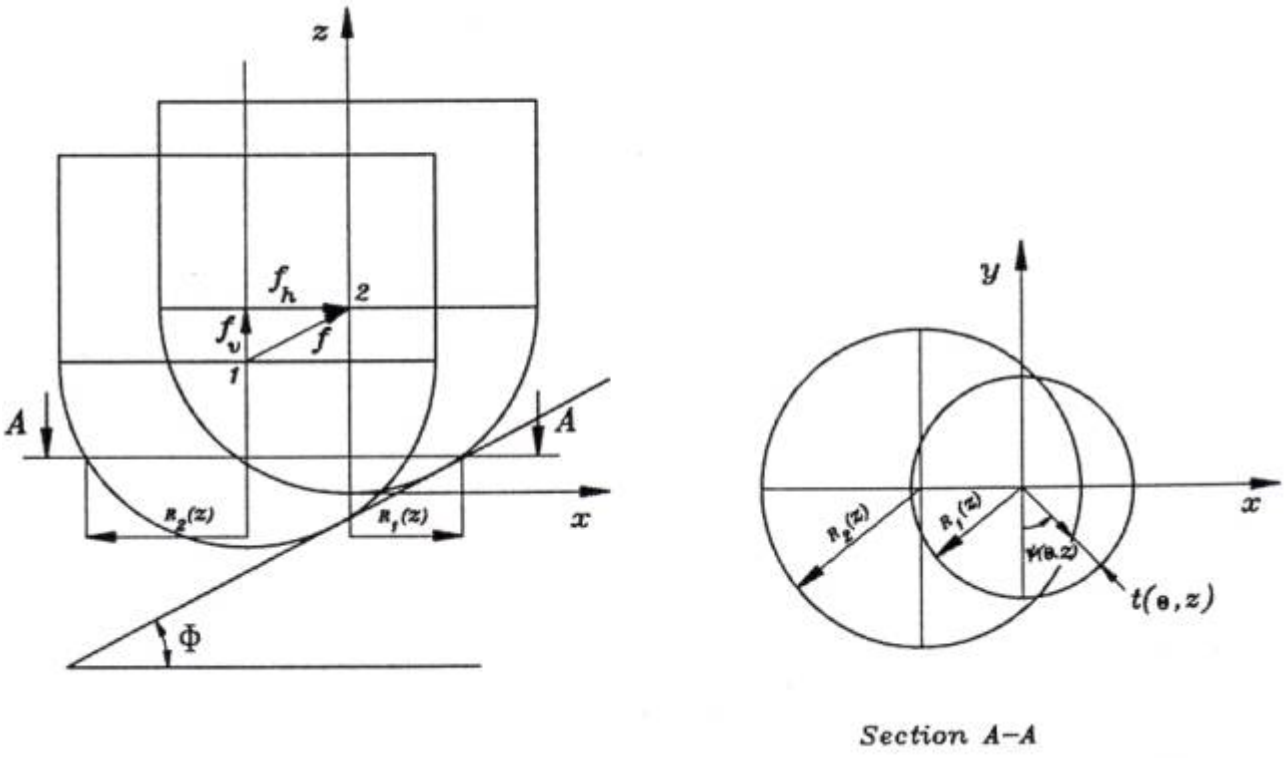

Figure 5. Chip thickness in three-dimensional ball-end milling process.

of the cutting edge (in-cut segment) with updated part for each tool rotation step. In order to compute the immersion geometry, the solid modeling based simulator of ball-end milling process is developed. A commercial geometric solid modeler (ACIS) is used for extracting the in-cut segment. The tool solid model, the cutting edge curve and the updated part are represented by ACIS. The updated part is shown if Figure 6a and is constructed by performing a Boolean subtraction between the part and the tool swept volume.

The true swept volume is the volume generated by a translation sweeping motion of a solid of revolution, which has proposed by Wang [14]. For the case of ball-end milling the solid of revolution (i.e. cutter), consists of a cylinder and semi-sphere representing the envelope of rotating cutting edges on the cylindrical and spherical parts of the ball-end mill.

Immersion geometry is computed using the contact face between the ball-end mill and the updated part. The contact face includes all the information required to calculate immersion geometry. In ball-end milling process, the contact face has three edges (AB, BC and AC edges in Figure 6b). AB and BC are B-spline edges and AC is circular. Intersecting an inclined plane with the cutter ball nose generates the cutting edge. For each cutting edge rotation step, intersection points between the cutting edge and the edges of the contact face are computed (points P1 and P2 in Figure 6b). In-cut segment is the height of these points from tool tip. The intersection between cutting edge and AC curve identifies lower engagement height (z_l) and the intersection between cutting edge and BC identifies upper engagement height (z_u).

3. PREDICTION OF MILLING FORCES

The unified mechanics of cutting approach introduced by Budak et al. [8] is extended to the ball-end milling process. It is assumed that the cutting edge is sharp and therefore the edge forces are not considered. The elemental tangential, dF_t, radial, dF_r, and axial, dF_a forces acting on an element in

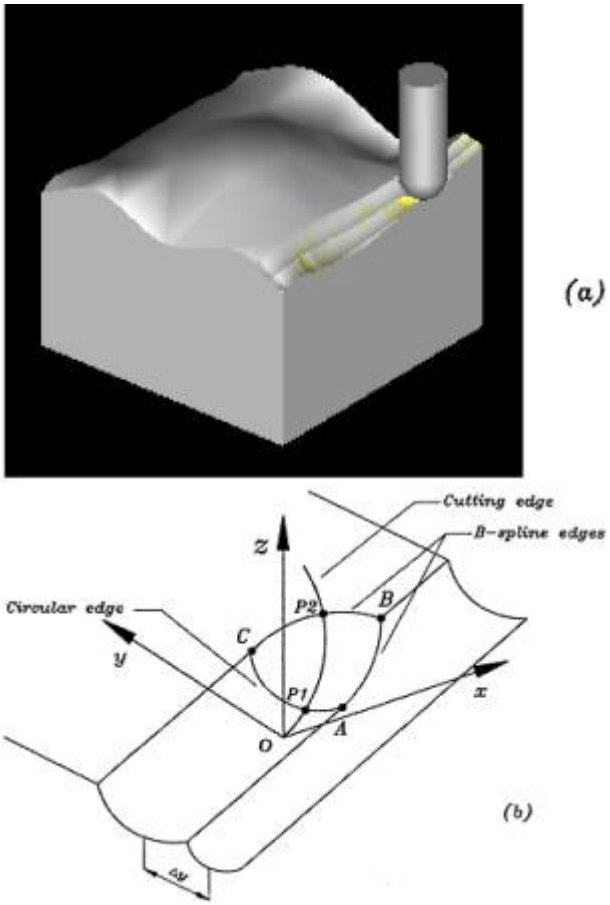

Figure 6. (a) Updated part (b) In-cut segment.

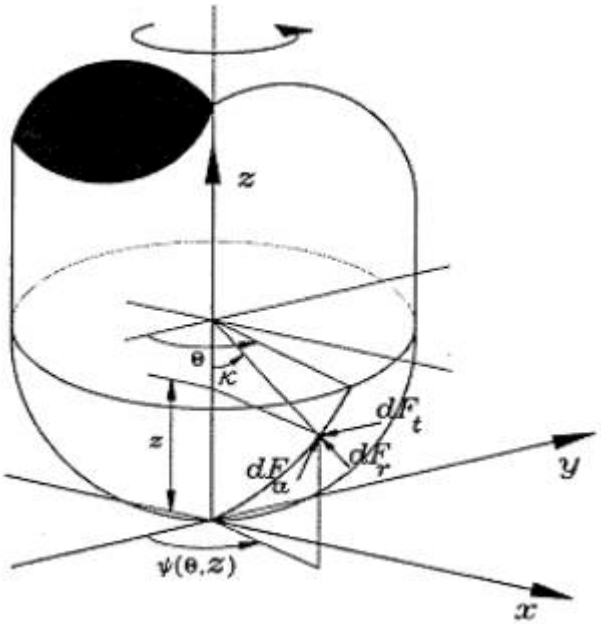

Figure 7. Elemental cutting force components acting on the cutting edge.

axial location z are given by (see Figure 7):

$$dF_t = K_t t_n(\theta, z)db$$

$$dF_r = K_r t_n(\Theta, z)db$$

$$dF_a(\Theta, z) = K_a t_n(\Theta, z)db \tag{18}$$

where $db = \frac{dz}{\cos\kappa}$, $\kappa = \arcsin\frac{R(z)}{R}$

and $t_n(\Theta, z) = t(\Theta, z)\sin\kappa$.

The cutting coefficients K_t, K_r and K_a are identified from a set of orthogonal cutting tests using an oblique transformation method[5]. The shear stress (τ), friction angle (β) and shear angle (ϕ) are modelled using the following equations[2]:

$$\tau = 1.586(vf)^{-0.25} + 67.7.3$$

$$\phi = 106.7(vf)^{0.5} + 0.375\alpha_e + 13.64$$

$$\beta = 48.4(vf)^{0.125} + 28.586 - \phi + \alpha_e \tag{19}$$

The differential cutting forces calculated using Equation 18 transformed to Cartesian coordinates as follows:

$$dFx = -\sin\kappa\sin\psi(\Theta, z)dF_r - \cos\psi(\Theta - z)dF_t + \cos\kappa\sin\psi(\Theta - z)dF_a$$

$$dF_y = \sin\kappa\cos\psi(\Theta - z)dF_r - \sin\psi(\Theta - z)dF_t - \cos\kappa\cos\psi(\Theta - z)dF_a$$

$$dF_z = \cos\kappa dF_r + \sin\kappa dF_a \tag{20}$$

Finally, the instantaneous cutting forces acting on the cutting edge can be expressed as:

$$\{F_x, F_y, F_z\} = \int_{z_l}^{z_u} dF_x, dF_y, dF_z \tag{21}$$

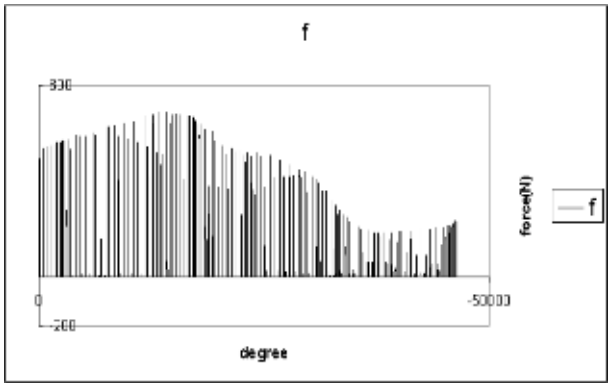

Figure 8. The variation of computed cutting forces for a sculptured surface.

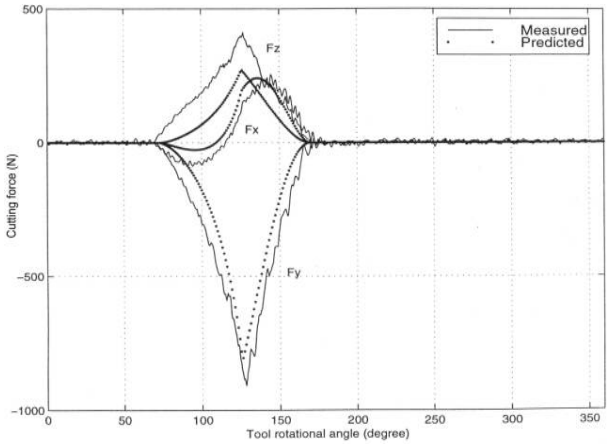

Figure 9. Predicted and measured cutting force components for $\Phi = 15^{\circ}, \Psi = 0^{\circ}$, Cutting conditions: spindle speed = 600 rpr, Feed = 48 $mm/\min$, Depth of cut = 2 mm and $\Delta y = 2mm$.

The integration limits (z_l and z_u) are the lower and upper boundaries of the in-cut segment and are provided by geometric simulation.

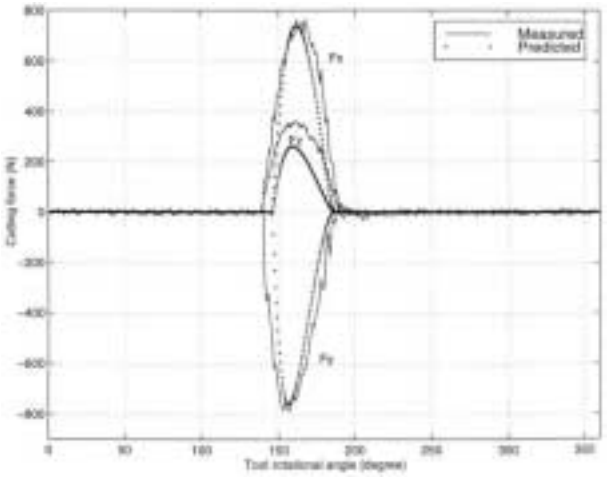

Figure 10. Predicted and measured cutting force components for $\Phi = 0^{\circ}, \Psi = 35^{\circ}$, Cutting conditions: spindle speed=600 rpm, Feed=48 $mm/\min$, Depth of cut=2 mm and $\Delta y = 2mm$.

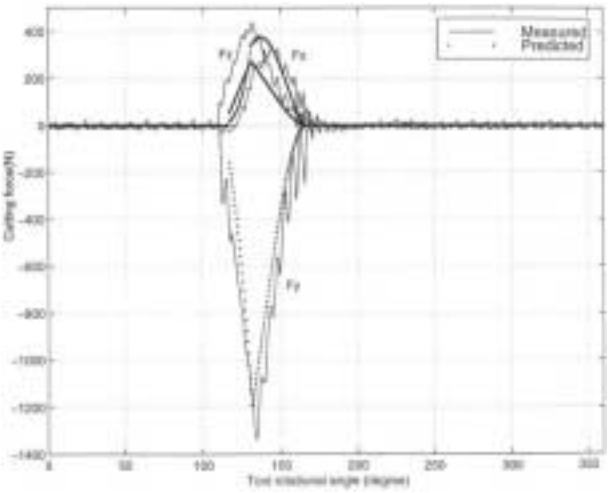

Figure 11. Predicted and measured cutting force components for $\Phi = 30^{\circ}, \Psi = 20^{\circ}$, cutting conditions: spindle speed = 600 rpm, Feed = 48 mm/min, Depth of cut = 2 mm and $\Delta y = 2mm$.

4. EXPERIMENTS AND RESULTS

Ball-end milling experiments using a 3-axis CNC milling machine were performed in order to verify the model simulation results. A 16 mm diameter, 20° rake angle, 1 flute ball-end mill was used in the experiments. The workpiece material was steel AISI 1045. The feed direction was along x axis and down milling operation was used. Instantaneous cutting forces were measured using a Kistler type 9255A, 3-D force component table dynamometer. The workpiece surfaces had two angles; one angle

relative to the x direction (Φ) and the other angle relative to the y direction (Ψ) (see Figure 1b). For any arbitrary point on the sculptured surface, a plane, which its two angles are the same as the workpiece angles are chosen, and the cutting forces are computed. The variation of computed cutting forces for a given sculptured surface is shown in Figure 8 and the predicted and measured cutting forces are shown in Figure 9 to Figure 11. The experiments indicate that the predicted forces agree reasonably well with the experimental results.

5. CONCLUSIONS

This paper represents an instantaneous rigid force model for prediction of cutting forces during ball-end milling of sculptured surfaces. The cutting edge and updated part geometry are modeled using a commercially available geometric modeler (ACIS). Intersecting an inclined plane with the cutter ball nose generates the cutting edge. The in-cut segments are extracted and are used by force model. The cutting forces generated by each element on the portion of the engaged cutting edge are evaluated by applying classical oblique cutting transformation to orthogonal cutting data. The total cutting force components for each tool rotation step are calculated by summing up the differential cutting forces.

The use of a "unified mechanics of cutting approach" to the prediction of ball-end milling forces, allows the model to be extended to any cutter geometry without milling calibration tests.

A sculptured surface can be approximated by a set of elemental planar surfaces with two angles, one angle relative to *x* direction, Φ, and the other angle relative to y direction, Ψ. Therefore for each block of NC tool path data, Φ and Ψ angles can be calculated and the cutting forces can be predicted using the proposed model.

6. NOMENCLATURE

x, y, z	Cartesian co-ordinates
dz	Differential length in axial direction
db	Differential cutting edge length in the direction perpendicular to the cutting velocity
dF_t, dF_r, dF_a	Differential cutting forces in tangential, radial, and axial directions
F_x, F_y, F_z	Total forces in Cartesian co-ordinates
K_t, K_r, K_a	Tangential, radial, and axial cutting force coefficients
f	Feed per tooth
R	Ball radius
i	Inclination angle or local helix angle
$i(z)$	Inclination angle at axial location *z*
$R(z)$	Cutter radius in $x-y$ plane at
$R(z)$	Axial location *z*
r	A vector in Cartesian co-ordinate from reference point to a point on the cutting edge
$t(\theta, z)$	Chip thickness at tool rotational angle θ and at axial location *z*
$t_n(\theta, z)$	Normal chip thickness in tool rotational angle θ and at axial location *z*
η_c	Chip flow angle
θ	Tool rotation angle about *z* axis
$\theta(z)$	Angle between ball tip $(z=0)$ and an element at axial location *z*
θ_o	Maximum angle between ball tip $(z=0)$ and an element at axial location $(z=R)$
$\psi(\theta, z)$	The angle of an element of cutting edge in global co-ordinate system
τ	Shear stress on shear plane
ϕ	Shear angle
β	Friction angle
β_n	Normal friction angle
α_n	Normal rake angle
α_e	Effective rake angle
N	Numbers of teeth
n	Spindle speed
z_l	Lower axial location of cutting edge engagement
z_u	Upper axial location of cutting edge engagement
Φ	Tilt angle of machined plane relative to x

direction

Ψ Tilt angle of machined plane relative to y direction

7. ACKNOWLEDGMENT

The authors would like to thank Professor M.A. Elbestawi of the McMaster University, Canada for providing experimental facilities.

8. REFERENCES

1. Bertok, P., "A System for Monitoring the Machining Operation by Referring to a Predicted Torque Pattern", ***CIRP Annals***, 32, (1983), 439-442.
2. El-Mounayri, H., Spence, A. D. and Elbestawi, M. A., "Enhanced CAD/CAM for Simulation and Optimization of 3-5 Axis Milling of Dies and Moulds", ***Proceedings of CSME 13th Symp. on Eng. Applications of Mechanics: Manufacturing Science and Engineering***, McMaster University, Canada, (1996), 394-401.
3. Spence, A. D., "Solid Modeller Based Milling Process Simulation", Ph. D. Thesis, The University of British Columbia, Canada, (1992).
4. Takata, S., "A Cutting Simulation System for Machinability Evaluation Using a Workpiece Model", ***CIRP Annals***, 38, (1989), 417-420.
5. Wang, W. P., "Application of Solid Modeling to Automate Machining Parameters for Complex Parts", ***Manufacturing Systems***, Vol. 7, No. 1, (1988), 57-63.
6. Yang, M. and Park, H., "The Prediction of Cutting Force in Ball-end Milling", ***Int. J. Mach. Tools Manufact.***, Vol. 31, No. 1, (1991), 45-54.
7. Feng, H. Y. and Menq, C. H., "The Prediction of Cutting Force in the Ball-end Milling Process-I. Model Formulation and Model Building Procedure", ***Int. J. Mach. Tools Manufact.***, Vol. 34, No. 5, (1994), 697-710.
8. Abrari, F., Elbestawi, M. A., "Closed Form Formulation of Cutting Forces for Ball and Flat End Mills", ***Int. J. Mach. Tools Manufact.***, Vol. 37, No. 1, (1996), 17-27.
9. Yucessan, G. and Altintas, Y., "Prediction of Ball-end Milling Forces", ***ASME J. of Eng. for Industry***, Vol. 118, (1996), 95-103.
10. Lee, P. and Altintas, Y., "Prediction of Ball-End Milling Forces from Orthogonal Cutting Data", ***Int. J. Mach. Tools Manufact.***, Vol. 36, No. 9, (1997), 1059-1072.
11. Imani, B. M., Sadeghi, M. H. and Elbestawi, M. A., "An Improved Process Simulation for Ball-end Milling of Sculptured Surfaces", ***Int. J. Mach. Tools Manufact.***, Vol. 38, (1998), 1089-1107.
12. ACIS Geometric Modeler Application Guide, Special Technology Inc., Colorado, USA, (1975).
13. Shaw, M. C., "Metal Cutting Principles", Clarendon press, Oxford, (1984).
14. Tlusty, J. and Ismail, F., "Special Aspects of Chatter in Milling", ***ASME Journal of Vibration, Stress and Reliability in Design***, Vol. 105, (1983), 24-32.
15. Lim, E. M., Feng, H. Y., Menq, C. H. and Lin, Z. H., "The Prediction of Dimensional Error for Sculptured Surface Productions Using the Ball-end Milling Process, Part 1: Chip Geometry Analysis and Cutting Force Prediction", ***Int. J. Mach. Tools Manufact.***, Vol. 35, No. 8, (1995), 1149-1169.
16. Budak, H., Altintas, Y. and Armarego, E. J., "Prediction of Milling Force Coefficients from Orthogonal Cutting Data", ***J. of Manufacturing Science and Engineering***, Vol. 118, May (1996).
17. Abrari, F., Elbestawi, M. A. and Spence, A. D., "On the Dynamics of Ball-end Milling Modeling of Cutting Forces and Stability Analysis", ***Int. J. Mach. Tools Manufact.***, Vol. 38, No. 3, (1998), 215-237.
18. Altintas, Y. and Lee, P., "Mechanics and Dynamics of Ball End Milling", ***ASME J. Manufact. Science and Eng.***, Vol. 120, (1998), 684-691.
19. Altintas, Y. and Chan, P. K., "In-Process Detection and Suppression of Chatter in Milling", ***Int. J. Mach. Tools Manufact.***, Vol. 32, No. 3, (1992), 329-347.
20. Ismail, F., Elbestawi, M. A., Du, R. and Urbasik, K., "Generation of Milled Surfaces Including Tool Dynamic and Wear", ***ASME J. Eng. For Industry***, Vol. 116, (1992), 435-439.
21. Wu, D. W., "A New Approach of Formulating the Transfer Function for Dynamic Cutting Processes", ***ASME J. of Eng. for Industry***, Vol. 111, (1989), 37-47.